Journal Pre-proof

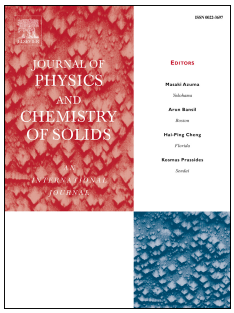

Cascade electron transfer in ternary CuO/α-Fe_2O_3/γ-Al_2O_3 nanocomposite as an effective visible photocatalyst

Aisha Kanwal, Shamaila Sajjad, Sajjad Ahmed Khan Leghari, Zameela Yousaf

PII: S0022-3697(20)32799-2

DOI: https://doi.org/10.1016/j.jpcs.2020.109899

Reference: PCS 109899

To appear in: *Journal of Physics and Chemistry of Solids*

Received Date: 5 July 2020

Revised Date: 30 October 2020

Accepted Date: 10 December 2020

Please cite this article as: A. Kanwal, S. Sajjad, S.A. Khan Leghari, Z. Yousaf, Cascade electron transfer in ternary CuO/α-Fe_2O_3/γ-Al_2O_3 nanocomposite as an effective visible photocatalyst, *Journal of Physics and Chemistry of Solids*, https://doi.org/10.1016/j.jpcs.2020.109899.

Credit author statement

Aisha Kanwal: Conceptualization, Methodology, Data curation, Writing- Original draft preparation

Shamaila Sajjad: Supervision, Validation, Resourses, Project administration

Sajjad Ahmed Khan Leghari: Visualization, Investigation, Writing- Reviewing and Editing

Zameela Yousaf: Writing- Reviewing and Editing

Graphical Abstract

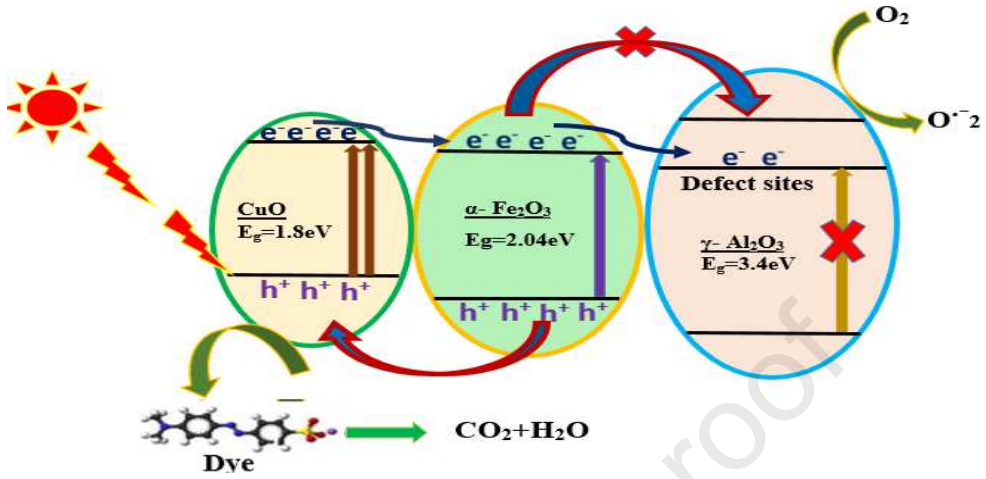

Cascade electron transfer in ternary CuO/α-Fe_2O_3/γ-Al_2O_3 nanocomposite as an effective visible photocatalyst

Aisha Kanwal[a], Shamaila Sajjad[a*], Sajjad Ahmed Khan Leghari[b], Zameela Yousaf[a]

[a] International Islamic University, H-10 Islamabad, Pakistan

[b] Pakistan Institute of Engineering and Applied Sciences, Islamabad, Pakistan.

Corresponding author e-mail. shalisajjad@yahoo.com

Corresponding Author Address: Associate Professor Faculty of Basic and Applied Sciences, International Islamic University Islamabad. 44000, Pakistan.

Phone No. 0092-51-9019813

Abstract

Highly efficient ternary heterojunction of CuO/α-Fe_2O_3/γ-Al_2O_3 was effectively fabricated by a facile and cost effective chemical route. The structural, chemical composition, morphology, optical and photocatalytic properties of as-prepared CuO/α-Fe_2O_3/γ-Al_2O_3 photo catalyst were compared to pristine and binary samples by various characterization. Existence of all the dominant peaks of CuO, α-Fe_2O_3 and γ-Al_2O_3 are noticeable in XRD spectrum of CuO/α-Fe_2O_3/γ-Al_2O_3 ternary photo catalyst which confirms the successful formation of the photocatalyst. SEM and HRTEM results revealed the spherical shape CuO nanoparticles with distorted α-Fe_2O_3 agglomerated plates which led to complete diffusion with γ-Al_2O_3. The band gap of ternary nanocomposite was found to be 1.9 eV elucidated by UV-DRS. Brunauer-Emmett-Teller (BET) analysis shown that due to the unique ternary nanocomposite structure and synergistic effect among various components, as-fabricated ternary CuO/α-Fe_2O_3/γ-Al_2O_3 nanocomposite exhibited the porous structure with large surface area and small pore volume as compared to pristine γ-Al_2O_3. The photocatalytic activity was examined by monitoring the deterioration of methyl orange under simulated solar light irradiation. CuO/α-Fe_2O_3/γ-Al_2O_3 exhibited superior photocatalytic efficacy as compared to CuO/γ-Al_2O_3 and α-Fe_2O_3/γ-Al_2O_3 binary and pure oxides of γ-Al_2O_3, CuO and α-Fe_2O_3. The marvelous photocatalytic activity of CuO/α-Fe_2O_3/γ-Al_2O_3 ternary nanocomposite samples can be ascribed to their close contact, strong interfacial hybridization and proficient charge transfer capacity. The electrochemical studies such as linear sweep voltammetry (LSV) and cyclic voltammetry (CV) were carried out to explore the charge transfer behavior and to support the high photo activity of ternary nanocomposite CuO/α-Fe_2O_3/γ-Al_2O_3. LSV measurements manifested that CuO/α-Fe_2O_3/γ-Al_2O_3 exhibited 4.3 folds higher current density than bare γ-Al_2O_3 which confirmed the faster

electron transfer from CuO to γ-Al_2O_3 via mediated α-Fe_2O_3 through the interfacial potential gradient in conduction band. Cyclic voltammetry (CV) results shown that pair of anodic and cathodic peaks in CuO/α-Fe_2O_3/γ-Al_2O_3 which affirm the efficient increase in photo-induced e^-/h^+ separation and suppress recombination rate of electron-hole pair. This work demonstrated that CuO/α-Fe_2O_3/γ-Al_2O_3 ternary nanocomposite found to be a promising candidate as an efficient adsorbent for organic dye removal from waste water.

Keywords: CuO/α-Fe_2O_3/γ-Al_2O_3; Ternary composite; Interfacial charge transfer; Environmental remediation; Cascade electron transfer.

1. Introduction

In past few years, heterostructure semiconductor nanomaterials have captivated much consideration of reader due to its potential employment in environmental applications. Particularly, water becomes the main source of environmental pollution as it is the primary carrier of all contaminations such as heavy metals, carcinogenic dyes, pharmaceutical desolations and industrial wastes [1, 2]. To combat such issues, numerous approaches have been adopted to treat effluents from water and to develop various processes such as photo-Fenton, adsorption wet-air oxidation, Fenton, and electrochemical oxidation, ozonation, evaporation, photocatalytic purification, microwave catalysis and chemical process. On the other hand, each approach has some limitations which generally include infuriation of large amount of solid wastes and production of toxic byproducts [3-6]. Recently, heterogeneous catalysis is an environmentally amiable and cost efficacious technique to expedite harmful compounds (pollutants) into the effective and carbonaceous products [7, 8]. The basic principle of photo catalysis involves the creation of electron hole (e-h) pair in semiconductor under visible light irradiation [9]. The heterostructures with different band gap materials have been employed to improve photo generated charge carrier separation efficiency in photo catalysis [4, 10, 11].

Gamma aluminum oxide (γ-Al_2O_3) is a supporting catalyst in the field of catalysis due to photochemical inertness, marvelous thermal stability, exquisite surface characteristics and unique acidic features [12-15]. Even, there are few drawbacks in γ-Al_2O_3 such as its low photo response and recombination rate due to a wide band gap (7.0-9.5 eV). Numerous approaches have been established to enhance photocatalytic efficiency and tuned optical properties to increase the light absorption capacity of γ-Al_2O_3 toward visible light range and suppress e-h pair recombination during photoreaction. This is achieved by composite fabrication, doping by metals

and non-metals and addition of transition metals or coupling of γ-Al_2O_3 with narrow band gap materials. It is important to modify the band gap of γ-Al_2O_3 which results in improvement of sensing, electrical and photo catalytic properties [7, 16]. Major instance has been paid to the coupling of γ-Al_2O_3 with some materials that shows superior charge transport properties to enrich the photocatalytic performance by eliminating the agglomeration of semiconductor. Recently, it was reported that γ-Al_2O_3 have defect sites which could accept photo-induced electrons to suppress the rate of recombination of (e-h) thus enhanced the photocatalytic activity [17, 18]. In this regard, hematite (α-Fe_2O_3) and cupric oxide (CuO) have been chosen to couple with γ-Al_2O_3 for increasing the dispersion of active sites to promote surface area, improved charge carrier efficiency that enhanced the photocatalytic activity. Cupric oxide (CuO) is a p-type semiconductor which exhibits a small optical band gap of 1.3-2.0 eV [19]. On the other hand, α-Fe_2O_3 is an n-type semiconductor that has low band gap in the range of 1.9eV-2.2 eV has more absorbing ability of visible light. Under the ambient atmosphere, α-Fe_2O_3 is the most stable form of iron oxide which is extensively used in water treatments, catalysis, sensors and lithium ion batteries [20-22]. CuO and α-Fe_2O_3 are the promising photo catalyst that have been widely used for the photo deterioration of organic contaminations and harmful products. A profusion of reports revealed that there are many binary and ternary hybrid structures based on α-Fe_2O_3 and CuO such as CuO/Cu_2O [23], Ag/Fe_2O_3 [21], SiO_2 and TiO_2 modified Fe_2O_3 [24], ZnO/CuO [16], TiO_2/Al_2O_3[18], Fe_3O_4@Fe_2O_3/Al_2O_3 [22], g-C_3N_4/Al_2O_3[17], WO_3/NiO/Fe_2O_3 [25], CuO/CeO_2 [26] and CuO/Al_2O_3 [27] etc. Literature study revealed that binary and ternary heterojunctions have been prepared by adopting various synthetic routes. The main focus of this study is to adopt an effective wet chemical synthetic route with same concentration of each oxide to prepare a novel ternary CuO/α-Fe_2O_3/γ-Al_2O_3 photo catalyst with marvelous optical, structural

and morphological properties. The remarkable enhancement in photocatalytic performance towards methyl orange (MO) under sunlight irradiation is observed. This study elucidates that ternary nanocomposite of CuO/α-Fe_2O_3/γ-Al_2O_3 exhibits increased photocatalytic degradation as compared to pure oxide samples and respective binary composite. Current research explains that high photocatalytic efficiency of ternary nanocomposite can be accredited to the synergetic effect between defect sites of γ-Al_2O_3, CuO and α-Fe_2O_3 nanoparticles which further promotes the minor recombination of photo created holes and electrons, and increases the mobility of charge carriers. As per our knowledge, no study has described the utilization of ternary composite of CuO/α-Fe_2O_3/γ-Al_2O_3 as a photocatalyst with cascade electron transfer. This study meticulously explain the comprehensive methodologies which can improve the selectivity of photo catalysis for crucial industrial processes.

2. Experimental

2.1. Materials and method

Aluminium foil, Copper nitrate Cu $(NO_3)_2$, Ferrous chloride ($FeCl_3$), Sodium hydroxide (NaOH) and Methyl orange were obtained from Sigma Aldrich. All the chemicals were analytically pure (99.99%) and were used as received. The deionized water was employed for synthesis of all aqueous solutions.

2.2. Synthesis of Gamma Alumina (γ-Al_2O_3), Hematite (α-Fe_2O_3) and Cupric Oxide (CuO)

In first step, pure γ-Al_2O_3, Hematite (α-Fe_2O_3) and Cupric Oxide (CuO) were fabricated by facile wet chemical route using Aluminum foil, Iron chloride and Copper nitrate as precursors, respectively. Typically, 6.0 g of Aluminum foil, 5.0 g Iron chloride and 5.0 g Copper nitrate were separately deliquesce in 100 mL water and each solution was kept under robust stirring

until homogeneous mixtures were obtained. Now sodium hydroxide (NaOH) solution is added drop by drop to each solution. All suspensions were kept under fast stirring at 60 °C for 3 h until γ-Al_2O_3, Hematite (α-Fe_2O_3), Cupric Oxide (CuO) nanoparticles were formed. The γ-Al_2O_3, α-Fe_2O_3 and CuO precipitates were then obtained by centrifugation. Finally several washings were done with deionized water to adjust the optimum pH value and to eliminate the residual reactants. Consequently, the nanoparticles were desiccated at 40 °C for 7h and then followed by calcination of dried powder samples at 800 °C for 4 h (γ-Al_2O_3), 500 °C for 2h (CuO) and 300 ^{o}C for 5h (α-Fe_2O_3).

2.3. Synthesis of α-Fe_2O_3/γ-Al_2O_3 and CuO/γ-Al_2O_3 binary composites

The binary nanocomposite of α-Fe_2O_3/γ-Al_2O_3 and CuO/γ-Al_2O_3 were fabricated by chemical method. As prepared 0.5 g of CuO and 0.5 g of α-Fe_2O_3 nanopowders were deliquesce separately in 50 mL deionized water with the γ-Al_2O_3 (0.5 g) in both solutions. The suspensions were stirred vigorously for 1 h at 40 ^{o}C. The precipitates were then washed many time with double distilled water by centrifugation to eliminate the excess salts from both solutions. Finally, collected binary composites of α-Fe_2O_3/γ-Al_2O_3 and CuO/γ-Al_2O_3 precipitates were dried in vacuum oven at 50 ^{o}C for 4 h prior for characterization.

2.4. Synthesis of CuO/α-Fe_2O_3/γ-Al_2O_3 ternary composite

Wet chemical method was adopted for the formation of ternary nanocomposite CuO/α-Fe_2O_3/γ-Al_2O_3. In a typical synthesis route, 0.5 g γ-Al_2O_3, 0.5 g α-Fe_2O_3 and 0.5 g CuO were added to 100 mL of distilled water. The prepared solution was magnetically stirred for approximately 120 min at 40 ^{o}C. Finally, the product were collected by centrifugation and then dried in vacuum

oven at 50 ^{o}C for 4 h to get CuO/α-Fe_2O_3/γ-Al_2O_3 nano-powder. The synthesis of ternary nanocomposite is given in Scheme 1.

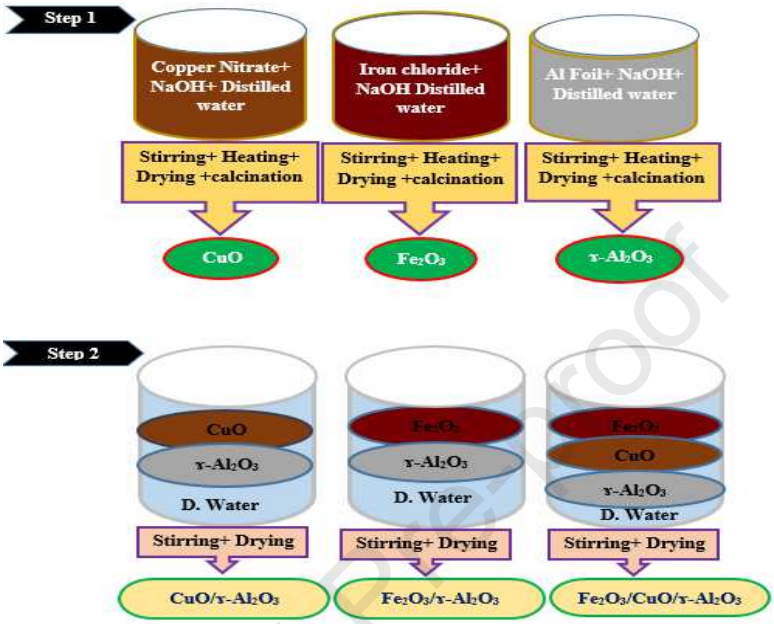

Scheme 1. Diagrammatic demonstration for the fabrication of CuO/α-Fe_2O_3/γ-Al_2O_3 ternary composite.

2.5. Material characterization

The crystallinity and crystal phase of prepared samples were analyzed by powder Rigaku D/MAX 2550 X-ray diffractometer using Cu Kα radiations (λ = 0.154056 nm) at ambient temperature in a broad range of Braggs angle from 10° to 80° operating at 30 mA with 40 kV. Surface features and textural properties of synthesized specimens were studied by Scanning Electron Microscopy (JEOL-JAD-2300). Energy Dispersive X-Ray (EDX) coupled with SEM was used to study the elemental configuration of as fabricated specimens. The structural morphologies of fabricated ternary nanocomposite was accomplished by a JEM-2100 (HRTEM) operated at an acceleration voltage of 200 kV. Fourier transform infrared spectroscopy was

employed to identify the functional groups and bond structures in the range of 400-4000 cm^{-1} by using FT-IR spectrometer of manufacturing model Nicolet 740. To examine the optical properties of fabricated specimens, Cary 100 UV-Vis spectrophotometer helps to collect the UV-Vis DRS spectra of prepared specimens with $BaSO_4$ as reflectance sample and a spectral reflectance standard is over a wavelength range from 200 to 700 nm. Kubelka-Munk function was employed to determine the optical band gap energies of prepared specimens. The electrochemical measurements were performed by using core test potentiostat.

2.6. Photocatalytic activity test

The photo activity of fabricated specimens was investigated by detoxification of methyl orange (MO) (toxic dye) upon exposure to solar light irradiation i.e visible light. All fabricated samples (0.05 g) were added into 50 mL of MO solution. The obtained solution was placed in dark and stirred for 30 min to achieve desorption/adsorption equilibrium of toxic dye methyl orange on the surface of ternary heterojunction of CuO/α-Fe_2O_3/γ-Al_2O_3. Then solution was irradiated for 4h under solar light to observe photocatalytic degradation efficiency. After the specific time period, a 5.0 mL of aliquot of the colloidal suspension was collected and centrifuged to separate the catalyst for further analysis. The clear transparent solution was then monitored by Schimadzu 2700 spectrophotometer in the range of 450-750 nm. The maximum absorption wavelength of MO at 464.0 nm.

3. Result and discussion

3.1. Characterization of as-prepared samples

The phase purity, crystalline structure and crystallite size of prepared samples were analyzed by X-ray powder diffraction technique. Figure 1(A) reveals the XRD pattern of as fabricated bare γ-

Al_2O_3, Hematite (α-Fe_2O_3) and Cupric Oxide (CuO). Fig. 1(B) depicts XRD profile of binary nanocomposites (α-Fe_2O_3/γ-Al_2O_3, CuO/γ-Al_2O_3) and ternary heterojunction (CuO/α-Fe_2O_3/γ-Al_2O_3). Fig. 1A(a) shows the diffraction peaks of pure γ-Al_2O_3 which can be ascribed to the cubic structure of γ-Al_2O_3 (JCPDS No. 10-0425) and the 2θ value along with the hkl values are 32.0^o (220), 37.5^o (311), 39.0^o (222), 46.0^o (400) and 67.0^o (440). The broad peaks shows the amorphous nature and low crystalline degree of γ-Al_2O_3 [7, 28]. The mean crystallite size of γ-Al_2O_3 has been computed by Debye Scherer formula and is found to be approximately 9.0 nm.

Fig. 1A (b) shows XRD photograph of Fe_2O_3 nanoparticles confirming the hematite phase (α-Fe_2O_3). The clearly prominent characteristic peak of α-Fe_2O_3 indexed at 2θ value of 23.7^o, 32.0 ^{o}, 36.0 ^{o}, 40.0 ^{o}, 49.0 ^{o}, 53.6 ^{o}, 62.0 ^{o} and 63.0 ^{o} corresponds to the crystal planes (012), (104), (110), (113), (024), (116), (214) and (300) which coincides well with JCPDS No. 39-1346. The average particle size of the fabricated NPs is ~14.0 ± 3.0 nm [29]. In case of pure CuO, it has two main peaks at the 35.2^o and 38.3^o associated to (-111) and (111) diffraction crystal planes as displayed in Fig. 1A (c). The other characteristics peaks appeared at 32.3^o (110), 48.8^o (-202), 53.2^o (020), 57.9^o (202), 61.3^o (-113), 66.0^o (022), 67.9^o (220) and 75.2^o (203) affirming fabrication of CuO nanoparticles with single monoclinic phase (JCPDS No. 045-0937) as no peaks of contaminations or other forms of CuO are observed. The intensity or sharpness of the peaks indicate the high degree of crystallinity of synthesized CuO nanoparticles [30, 31]. No impurity and remnant peaks have been observed in all three pure samples which manifests the high grade purity of synthesized samples. The average particle size of CuO is approximately 8.0±2.0 nm. Figure 1B(a) illustrates that the XRD pattern of binary CuO/γ-Al_2O_3 nanocomposite implicate that all the main peaks of bare CuO and γ-Al_2O_3 exists in the pattern confirming the successful formation of CuO/γ-Al_2O_3. No peak shift has been observed which shows the stability of binary

structure. XRD pattern of α-Fe_2O_3/γ-Al_2O_3 nanocomposite is depicted in Fig. 1B (b). The peak appeared at 2θ=46.0^o and 67.0^o is ascribed to γ-Al_2O_3 (JCPDS card 29-0063) whereas much diminished peak of α-Fe_2O_3 has been observed in binary nanocomposite. The main reason for disappearance of α-Fe_2O_3 in α-Fe_2O_3/γ-Al_2O_3 is the encapsulation of α-Fe_2O_3 crystallites by γ-Al_2O_3. Thus, X-ray diffraction peak of α-Fe_2O_3 is insignificant in hybrid structure of α-Fe_2O_3/γ-Al_2O_3 [32, 33]. Figure 1B (c) displays the diffraction pattern of CuO/α-Fe_2O_3/γ-Al_2O_3 ternary nanocomposite. The heterostructure CuO/α-Fe_2O_3/γ-Al_2O_3 is composed of three kinds of phases, cubic γ-Al_2O_3, α-Fe_2O_3 and monoclinic CuO confirming the successful formation of the ternary heterostructure. On the other hand, there was no prominent peak shift as well as no other impurities were found and no traces of other phases were spotted, suggesting the high purity of the samples and confirming that CuO, α-Fe_2O_3 and γ-Al_2O_3 coupled together successfully and without other phases.

The existence of defect sites in γ-Al_2O_3 can be justified by the results obtained from the XRD. XRD results as depicted in Fig. 1 clearly displays the broad peaks at 47.0^o and 67.0^o in all synthesized samples (pristine, binary and ternary nanocomposites). The broadening of peaks describes the low degree of crystallinity and the indication of amorphous structure. Amorphous structure of γ-Al_2O_3 possess a lot of surface active sites and defects which are responsible for capturing the electrons more effectively in hybrid system [28].

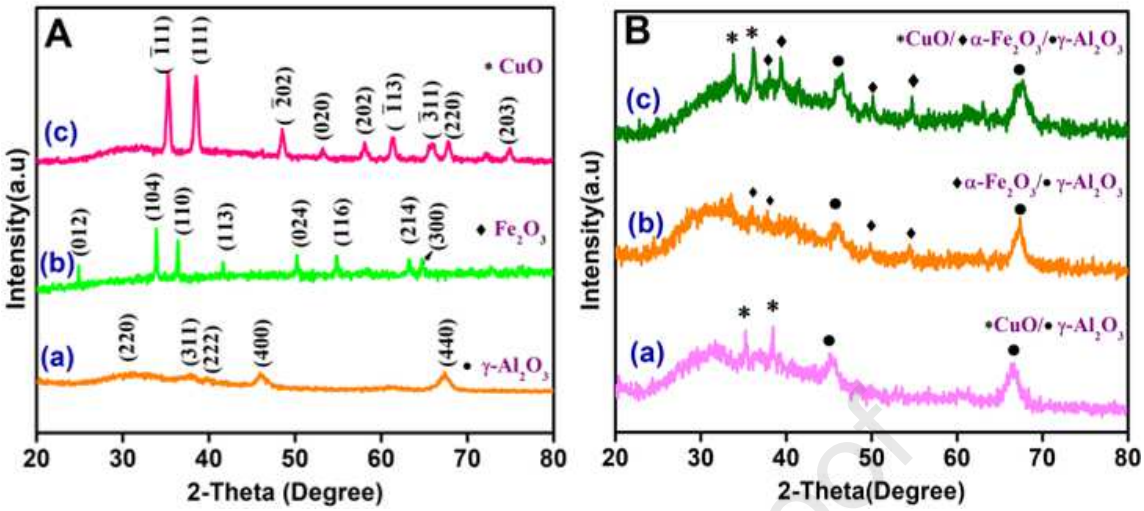

Figure 1. (A) XRD diffraction patterns of pristine oxides, binary and ternary nanocomposites; (a) γ-Al_2O_3 (b) α-Fe_2O_3 (c) CuO; (B) (a) CuO/γ-Al_2O_3 (b) α-Fe_2O_3/γ-Al_2O_3 (c) CuO/α-Fe_2O_3/γ-Al_2O_3.

The surface morphology of nanomaterials and their ternary nanocomposite CuO/α-Fe_2O_3/γ-Al_2O_3 were examined by scanning electron microscope. Figure 2 depicts the SEM photographs of bare γ-Al_2O_3, α-Fe_2O_3, CuO and ternary heterostructure synthesized with same concentration of each oxide. Figure 2A illustrates the dispersed leafy morphology of pure γ-Al_2O_3. Figure 2B demonstrates that pure CuO has spherical morphology with uniform distribution [34]. Irregular plate like architect with smooth surface are observed for pure α-Fe_2O_3 with small agglomeration as shown in Fig. 2C [35]. Textural features of ternary heterostructure CuO/α-Fe_2O_3/γ-Al_2O_3 are manifested in Fig. 2D. It can clearly be seen that ternary nanocomposite consists of spherical particles and plate like morphology. CuO and α-Fe_2O_3 are well incorporated with Al_2O_3 matrix and decorated on surface of γ-Al_2O_3. This promotes the intimate interfacial connection between them to provide the more active sites for maximum degradation of dye molecule to enhance photocatalytic performance.

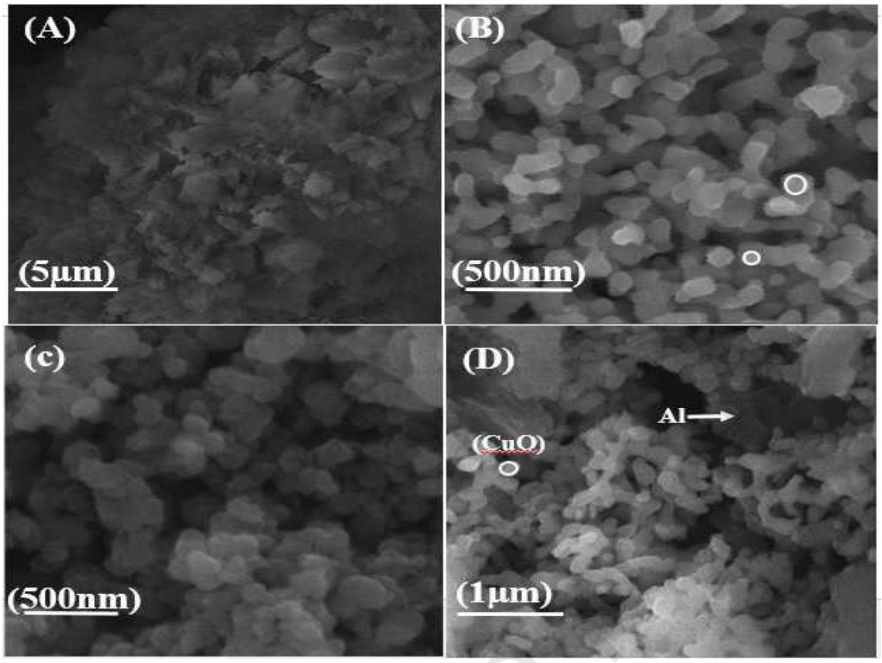

Figure 2. SEM images of as-prepare samples; (A) γ-Al_2O_3, (B) CuO, (c) α-Fe_2O_3, and (D) CuO/α-Fe_2O_3/γ-Al_2O_3.

Fourier transform infrared spectroscopy evidenced the various surfaces functional groups and confirmed the chemical structure of as-prepared samples. Figure 3 (A-D) exhibits the FT-IR spectra for pure γ-Al_2O_3, binary heterojunctions (α-Fe_2O_3/γ-Al_2O_3, CuO/γ-Al_2O_3) and ternary nanocomposite of CuO/α-Fe_2O_3/γ-Al_2O_3. Figure 3A depicts the FTIR spectra of γ-Al_2O_3. The peaks between 500-800 cm^{-1} is attributed to the γ-Al_2O_3. The most evident peak at 645 cm^{-1} is assigned to the stretching vibrational mode of Al-O. The peak appeared at 1000-1032 cm^{-1} is ascribed to Al-O bending vibrational mode. A peak at 1062 cm^{-1} is corresponding with symmetrical bending mode of Al-O-H group [36- 38]. FT-IR results of binary nanocomposite α-Fe_2O_3/γ-Al_2O_3 is given in Fig. 3B. It displays the characteristics peaks of α-Fe_2O_3 phase in the range of 400-700 cm^{-1}. The strong peak below the 700 cm^{-1} is accredited to Fe-O stretching mode. The strong and sharp bands appeared at 466 and 576 cm^{-1} are ascribed to Fe-O stretching

mode [39-42]. The intense peak occurred at 644 cm^{-1} can be associated to Al-O stretching vibration mode and a peak at 1041 cm^{-1} can be related with Al-O-H group [36-38, 43]. The bands ranging from 3300-3500 cm^{-1} is accredited to OH group and water molecules that are adsorbed on surface respectively [44]. The above mentioned peaks of both hematite (α-Fe_2O_3) and γ-Al_2O_3 confirmed the successful formation of binary nanocomposite α-Fe_2O_3/γ-Al_2O_3. Figure 3C demonstrates the FT-IR spectrum of CuO/γ-Al_2O_3 binary nanocomposite. The three main absorption peaks shows the vibrational mode of CuO in the range of 500-700 cm^{-1}. The dominant and sharp vibration peak for CuO was noticed at 434 cm^{-1} and the peak at 525 cm^{-1} linked to the stretching mode of CuO [45]. The band at 802 cm^{-1} can be assigned to Cu-OH [46]. The hump shown at 647 cm^{-1} is attributed to Al-O stretching mode in γ-Al_2O_3. The peak located at 1313 cm^{-1} may arise due to existence of CO_2 which usually resides on the surface of sample by adsorption from air or may be due to organic moieties [4]. These characteristic vibrations and bending modes reappear in the FTIR spectrum of the CuO/α-Fe_2O_3/γ-Al_2O_3 (Fig. 3D) which demonstrates successful formation of ternary nanocomposite. The peak occurred at 434 cm^{-1} to 525 cm^{-1} may be related to Cu-O stretching vibration mode [45, 47]. The band appeared at 879 cm^{-1} is associated to Cu-OH vibrational mode of CuO [46]. Fe-O stretching mode of α-Fe_2O_3 is observed at 446 cm^{-1} and 563 cm^{-1} [48, 49]. The γ-Al_2O_3 is confirmed in the ternary nanocomposite by the valley between 1000-400 cm^{-1} in the spectral range and the peak at 778 cm^{-1} corresponds to the vibrational bending of Al-O. The peak at 645 cm^{-1} can be accredited to Al-O-Al in γ-Al_2O_3 [50]. The band appeared in all FT-IR spectra in the range between 1200-2000 cm^{-1} arises due to organic moieties and bands in the range of 3300-3500 cm^{-1} is attributed to hydroxyl group as vibrational stretching from absorbed water molecules [4, 51].

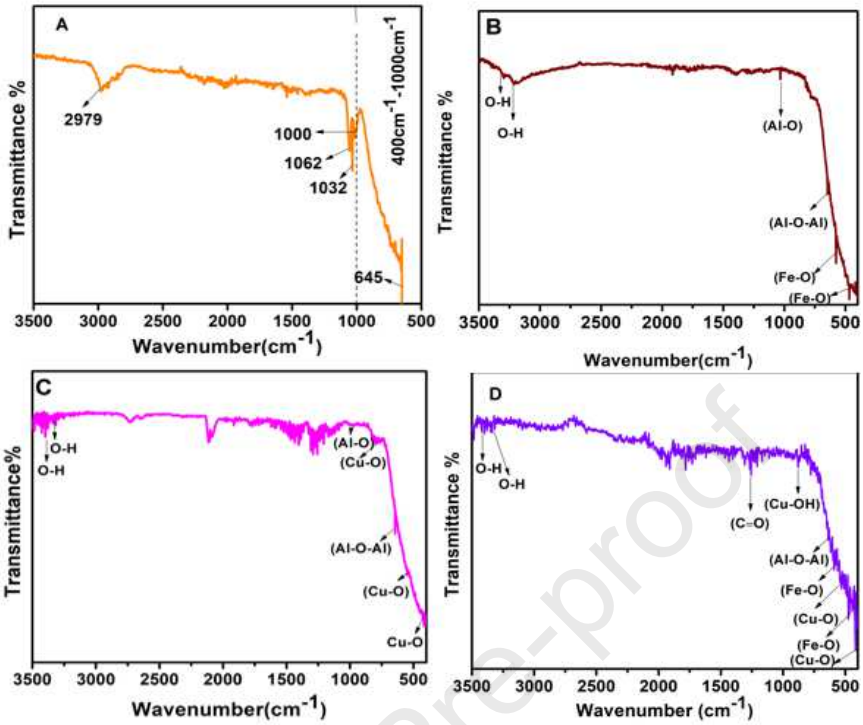

Figure 3. FT-IR of pristine oxides, binary and ternary composites (A) pure γ-Al_2O_3; (B) α-Fe_2O_3/γ-Al_2O_3; (C) CuO/γ-Al_2O_3; (D) CuO/α-Fe_2O_3/γ-Al_2O_3.

The elemental configuration and distribution of as synthesized materials were evaluated and affirmed by energy dispersive spectroscopy and is displayed in Fig. 4(A-D). Figure 4A shows the existence of Al and O in bare sample of γ-Al_2O_3. EDX spectra of binary heterojunction α-Fe_2O_3/γ-Al_2O_3 are illustrated in Fig. 4B. According to EDX pronounced peaks of Al, Fe and O elements are distinctly seen. In case of CuO/γ-Al_2O_3, the peaks are ascribed to Al, Cu and O without any impurity peaks as shown in Fig. 4C. X-ray elemental mapping profile of ternary nanocomposite (CuO/α-Fe_2O_3/γ-Al_2O_3) is shown in Fig. 4D and manifested the successful fabrication of pure-phase of ternary nano-hybrid structure by the existence of Fe, Cu, Al and O. Presence of all elements (Al, Cu, Fe and O) implies the uniform distribution over the surface of ternary hybrid structure. Moreover, no impurity peaks have been noticed in EDX spectra of all

synthesized samples which assure the purity of samples. Table 1 describes the relative configuration of prepared samples.

Table 1. Elemental composition of the fabricated specimens of pure oxides, binary and ternary composites.

Elements	γ-Al_2O_3		CuO/γ-Al_2O_3		α-Fe_2O_3/γ-Al_2O_3		CuO/α-$Fe_2O_3\gamma$-Al_2O_3	
	At. %	Wt. %	At. %	Wt. %	At. %	Wt. %	At. %	Wt. %
Al	33.04	45.42	34.49	42.35	32.74	43.83	31.76	38.69
Cu	------	------	4.59	13.29	-----	------	3.07	8.81
Fe	------	------	-----	-------	1.41	3.90	3.02	7.62
O	66.96	54.58	60.92	44.36	65.85	52.27	62.15	44.89
Total	100	100	100	100	100	100	100	100

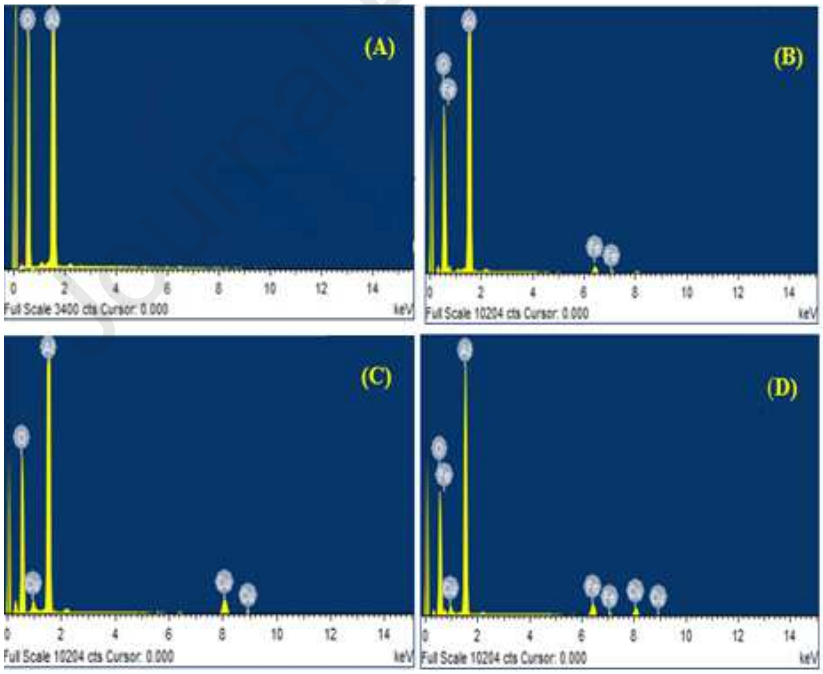

Figure 4. EDX analysis of (A) pristine γ-Al_2O_3; (B) α-Fe_2O_3/γ-Al_2O_3; (C) CuO/γ-Al_2O_3 and (D) CuO/α-Fe_2O_3/γ-Al_2O_3.

To study the optical properties and to probe the relationship between the electronic structures of synthesized samples, UV-Vis DRS of pure samples, binary and ternary nano-hybrid structures are depicted in Figure 5(A-F). Kubelka-Munk function helps to calculate the optical band gap energies of prepared samples. The Kubelka-Munk function is given as;

$$F(R) = K/S = (1-R)^2 / 2R$$

Where, R = reflectance of material, S = scattering coefficient, K= molar absorption coefficient.

It is approximated by drawing a tangent to the curve on to X-axis. Figure 5(A-C) illustrates the calculated band gaps to be 3.4 eV, 2.04 eV and 1.8 eV for pure samples of γ-Al_2O_3, α-Fe_2O_3 and CuO, respectively which coincided well with reported literature [7, 52, 53]. It can be seen that the addition of α-Fe_2O_3 and CuO influence the optical property of light absorption of binary and ternary heterostructure significantly. The band gap values of binary heterostructures are found to be 2.1 eV and 3.0 eV for α-Fe_2O_3/γ-Al_2O_3 and CuO/γ-Al_2O_3, respectively as demonstrated in Fig. 5(D, E). The calculated band gap energy value of as prepared γ-Al_2O_3 is 3.4 eV which is far smaller than previously reported for insulators >5.0 eV. The significantly low band gap value of γ-Al_2O_3 may be ascribed to surface defects in the γ-Al_2O_3 particles. This existence of defects can be associated with the hybridization of the sp^3 orbitals of γ-Al_2O_3 [7, 54]. The band gap narrowing of host material i.e γ-Al_2O_3 may be due to the intimate interfacial interaction which suggests that the combination of α-Fe_2O_3 and CuO nanoparticles with γ-Al_2O_3 which could probably make modifications to γ-Al_2O_3 in the basic process of e-h pair formation under sunlight illumination. The band gap of ternary nanocomposite CuO/α-Fe_2O_3/γ-Al_2O_3 is 1.9 eV which is calculated by transformed Kubelka-Munk function. From the results (Fig. 5F), it is clear that there is a remarkable narrowing in the band gap of the ternary heterostructure (CuO/α-Fe_2O_3/γ-Al_2O_3) in comparison with pure and binary samples. This may be ascribed to the synergic effect

of the composite constituent's i.e γ-Al_2O_3, CuO and α-Fe_2O_3 leading to strong interfacial interaction between constituents causing formation of new molecular orbitals of lower energy. Therefore, photocatalytic phenomena by ternary nanocomposite could be better than binary composite.

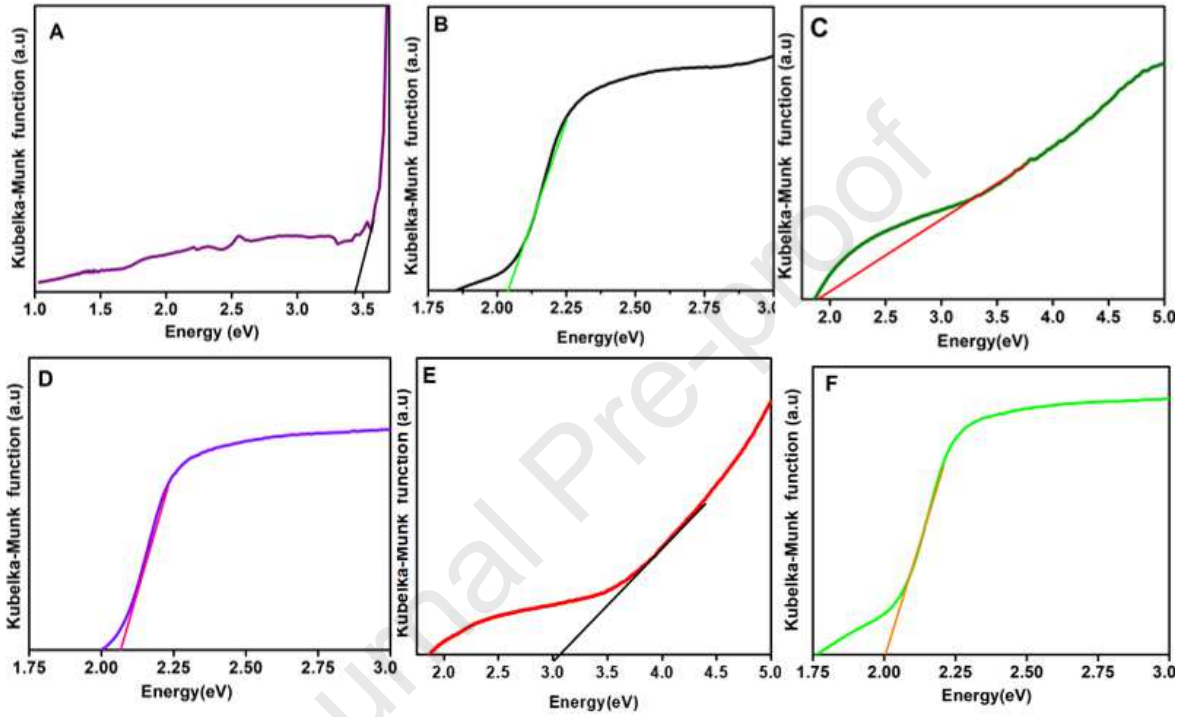

Figure 5. Kubelka-Munk function (KMF) of pure oxides, binary and ternary nanocomposites; (A) γ-Al_2O_3, (B) α-Fe_2O_3, (C) CuO, (D) α-Fe_2O_3/γ-Al_2O_3, (E) CuO/γ-Al_2O_3, (F) CuO/α-Fe_2O_3/γ-Al_2O_3.

To investigate the structure of CuO/α-Fe_2O_3/γ-Al_2O_3 ternary nanocomposite, TEM and HRTEM images of CuO/α-Fe_2O_3/γ-Al_2O_3 ternary nanocomposite at different resolutions are shown in Figure 6(A-C). Figure 6(A, B) displays TEM image of CuO/α-Fe_2O_3/γ-Al_2O_3 catalyst has a little distorted spherical shape and plate like morphology which is in accordance with SEM results. Cu, and Fe could be distinctly seen on the porous surface of γ-Al_2O_3 as well which evidenced the successful fabrication of ternary catalyst. From TEM photographs, it could be expected that an

intimate interfacial channel exist in CuO/α-Fe_2O_3/γ-Al_2O_3 ternary heterojunction, which would support the efficient charge carriers transfer thus causing enhancement in the photocatalytic activity. High resolution TEM image (HRTEM) in Fig. 6(C) exhibits lattice fringes of the CuO/α-Fe_2O_3/γ-Al_2O_3 ternary hybrid structure which have three major noticeable fringes with an inter planer spacing of 0.25, 0.23 and 0.33 nm, associated to the crystalline nature of α-Fe_2O_3, CuO coordinated with γ-Al_2O_3, respectively [53,24]. XRD results is in corroborate with the TEM results.

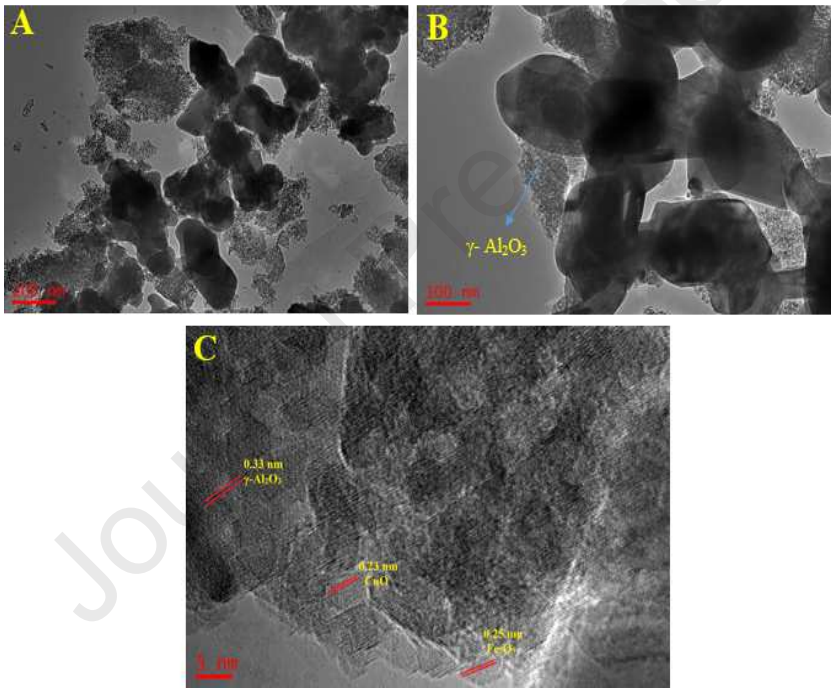

Figure 6. TEM (A, B) and HRTEM (C) images of ternary nanocomposite of CuO/α-Fe_2O_3/γ-Al_2O_3.

Cyclic voltammetry (CV) is a powerful technique to elucidate the redox behavior, electrochemical properties and electron transfer kinetics of prepared materials. The cyclic voltammetry analysis was performed at a scan rate of 10 mV/s in the potential range from 0.7 V to 1.6 V using 1.0 M of NaOH as electrolyte. Figure. 7 delineates the CV scan of pristine γ-

Al_2O_3 and CuO/α-Fe_2O_3/γ-Al_2O_3 ternary nanocomposites. Negligible current response and no redox peak have been found for bare γ-Al_2O_3 as shown in Fig. 7A. CuO/α-Fe_2O_3/γ-Al_2O_3 hybrid structure (Fig. 7B) possess maximum current for both forward and reverse scans. The existence of pair of particular redox (anodic and cathodic) peaks and significant increase in current density of the ternary nanocomposite may be accredited to the synergistic interaction of individual components in ternary nanocomposite which creates more number of catalytic sites and enhances electron transfer. Moreover, the enhancement in current density of CuO/α-Fe_2O_3/γ-Al_2O_3 suggested the existence of appropriate electronic channels between CuO, α-Fe_2O_3 and γ-Al_2O_3 to effectively increase the photo-induced e^--h^+ separation and simultaneously decreased the recombination rate of e^-/h^+ pair [55-57].

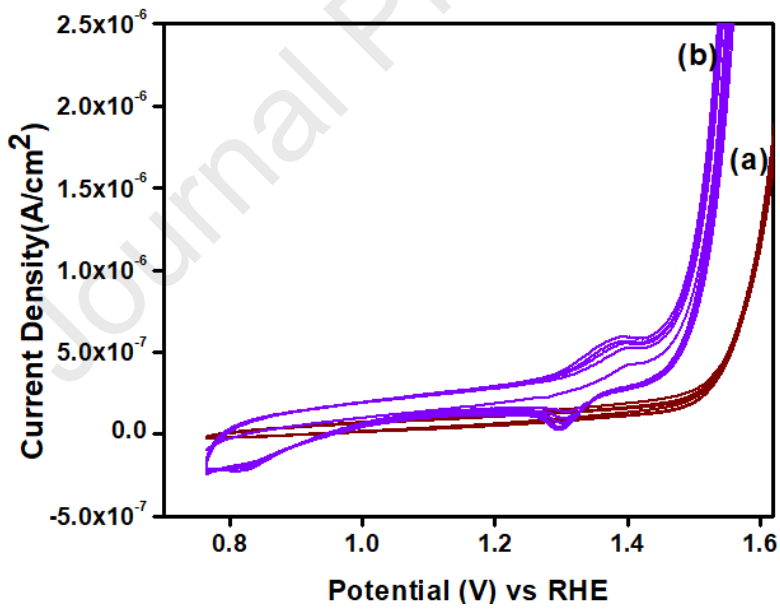

Figure 7. CV of pristine and ternary nanocomposite, (a) bare γ-Al_2O_3 (b) ternary nanocomposite of CuO/α-Fe_2O_3/γ-Al_2O_3 at scan rate of 10 mV s^{-1}.

Linear sweep voltammetry (LSV) helps to explain e^- and h^+ recombination rate and to study the transfer of photo induced charge carriers [58]. Figure 8 depicts the linear sweep voltammetry

(LSV) plots of pure γ-Al_2O_3 and ternary heterojunction CuO/α-Fe_2O_3/γ-Al_2O_3 was carried out at scan rate of 10 mV/s sweeping potential range from 0.7V to 1.8V in the 1M NaOH electrolyte solution. As presented in Fig. 8a, the current density of pristine γ-Al_2O_3 is very small. However, Fig. 8b illustrates that the inclusion of CuO and α-Fe_2O_3 to γ-Al_2O_3 significantly increases the current density which in turn effectively promotes the electron mobility of ternary photo catalyst CuO/α-Fe_2O_3/γ-Al_2O_3. This enhancement in photocurrent density affirmed the increase in transfer of photo generated charge carrier through interfacial hybridization and reduce the e^-/h^+ pair recombination. By interfacial transfer of charge, photocurrent density exhibited by ternary heterojunction is 69 μA/cm^2 at a potential of 1.76 V which is about 4.3 folds greater than those of the pure γ-Al_2O_3 (16 μA/cm^2). This supports that the efficient charge transfer occurs from CuO to Al_2O_3 via α-Fe_2O_3. The synergetic interaction of CuO and α-Fe_2O_3 with Al_2O_3 causes the increase in electron mobility (photocurrent) which provides more active site and hence resulting in excellent photocatalytic activity [56, 58].

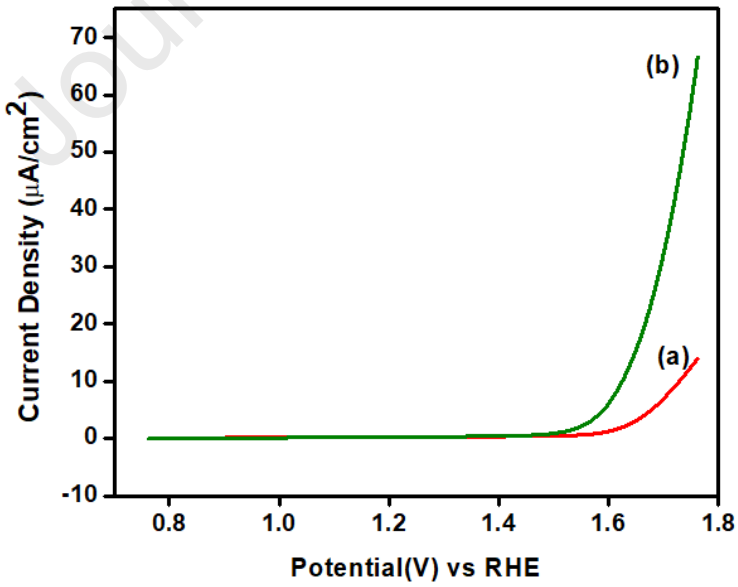

Figure 8. Linear sweep voltammetry curves of pristine and ternary composite, (a) pure γ-Al_2O_3 (b) CuO/α-Fe_2O_3/γ-Al_2O_3 at scan rate of 10 m/v.

In order to determine the surface area, pore volume and pore diameter of catalysts are performed by the N_2 adsorption-desorption isotherms [59]. The adsorption in porous materials may be attributed to the specific properties such as specific surface area, pore diameter and total pore volume of porous stricture [60]. The hysteresis loop of γ-Al_2O_3 and CuO/α-Fe_2O_3/γ-Al_2O_3 (Figure 9) at relative pressure (0.4-1.0) P/P_o represents the type II isotherm which further confirms the porous structure of nanomaterial. CuO/α-Fe_2O_3/γ-Al_2O_3 ternary nanocomposite shows the higher surface area 156.2 cm^2/g than pristine γ-Al_2O_3 (143.4 cm^2/g). Pore volume of pure γ-Al_2O_3 and α-Fe_2O_3/CuO/γ-Al_2O_3 is noted to be 0.0023 and 0.0020 cm^3/g respectively. High surface area, small pore volume and pore diameter of CuO/α-Fe_2O_3/γ-Al_2O_3 ternary hybrid structure exhibits that light may scatter efficiently and increase photo catalytic activity under visible light irradiation and rapid charge transfer ability in catalytic activity.

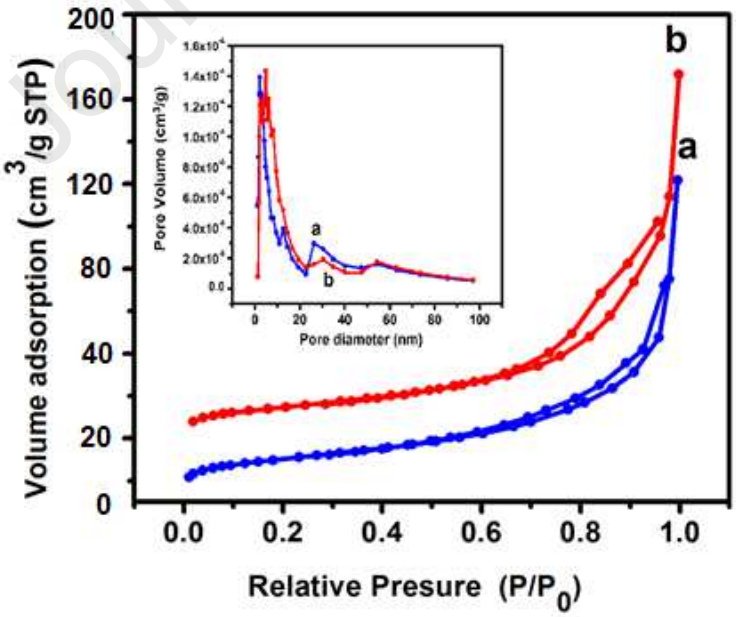

Figure 9. N_2 Adsorption desorption of (a) γ-Al_2O_3 and (b) CuO/α-Fe_2O_3/γ-Al_2O_3 at 77 K.

3.2. Photocatalysis

Methyl orange (organic pollutant) is used to assess the photocatalytic activity of synthesized specimens upon exposure to visible light. For comparison, the photo catalytic activity of the pure oxides, γ-Al_2O_3, α-Fe_2O_3 and CuO was also measured. The photocatalytic activity of pure oxide, binary and ternary nanostructures is manifested in Fig 10A. Prior to irradiation, the samples were placed in dark for half an hour to acquire adsorption-desorption equilibrium. As shown in Fig. 10Aa γ-Al_2O_3 alone show a very low photocatalytic activity 8.0%. This low photocatalytic activity is due to large band gap which makes it less effective harvester of solar light and that is the drawback of γ-Al_2O_3 for the use of sunlight [7]. Pure CuO shows 57.0% degradation of MO as clear from Fig. 10Ab. Earlier studies revealed that CuO nanoparticles show very low photo activity towards decomposition of MO and MB dyes. The reason for low decomposition efficiency of CuO under sunlight is the quick recombination of e-h pair due to very small band gap energy [53, 61]. Photocatalytic activity of bare α-Fe_2O_3 is shown in Fig. 10Ac and only 68.0% degradation of MO is observed. Pure α-Fe_2O_3 has photocatalytic activity which is limited by some features like fast recombination rate of e-h, poor conductivity and low diffusion lengths of holes which leads to low performance of iron oxide. These drawbacks of α-Fe_2O_3 can overcome by lowering the recombination rate by designing heterostructures that can cause increase in conductivity by coupling with suitable materials and increasing the charge transfer capability [62]. The coupling of γ-Al_2O_3 with α-Fe_2O_3 and CuO to form binary nanocomposites of α-Fe_2O_3/γ-Al_2O_3 and CuO/γ-Al_2O_3 shows improved photocatalytic performance of γ-Al_2O_3 as illustrated in Fig. 10A(d, e). α- Fe_2O_3/γ-Al_2O_3 exhibits better photocatalytic efficiency than CuO/γ-Al_2O_3 under sunlight irradiation. The appreciable photocatalytic performance of α-Fe_2O_3/γ-Al_2O_3 is due to synergetic effect between α-Fe_2O_3 and γ-Al_2O_3. The interfaces in the

heterojunction has a vital impact on supporting the overall photocatalytic performance of binary nanocomposite [52]. Furthermore, ternary CuO/α-Fe_2O_3/γ-Al_2O_3 nanocomposite (Fig. 10Af) exhibits higher degradation efficiency as compared to both binary nanocomposite (α-Fe_2O_3/γ-Al_2O_3 and CuO/γ-Al_2O_3) and pure samples under visible light irradiation. Under the sunlight, ternary nanocomposite degraded approximately 98.0% of MO. While α-Fe_2O_3/γ-Al_2O_3 and CuO/γ-Al_2O_3 nanocomposites degraded only 92.0% and 85.0% of MO, respectively. This increase in MO degradation efficiency using ternary heterostructure is attributed to the existence of the interfaces between CuO, α-Fe_2O_3 and γ-Al_2O_3. Photocatalytic oxidation reduction reaction occurs on the surface of photo catalyst and significantly makes surface properties better which in turn influence the performance of catalyst [5]. The synergetic effect of CuO, α-Fe_2O_3 in γ-Al_2O_3 structure in the degradation of MO is associated to these species in suppressing electron hole recombination rate and improving the reactive species [63]. Consequently, the superb CuO/α-Fe_2O_3/γ-Al_2O_3 photo catalyst is much more effective under solar light due to two main reasons; (1) strong optical absorbance property, (2) large surface area of ternary nanocomposite [7, 64].

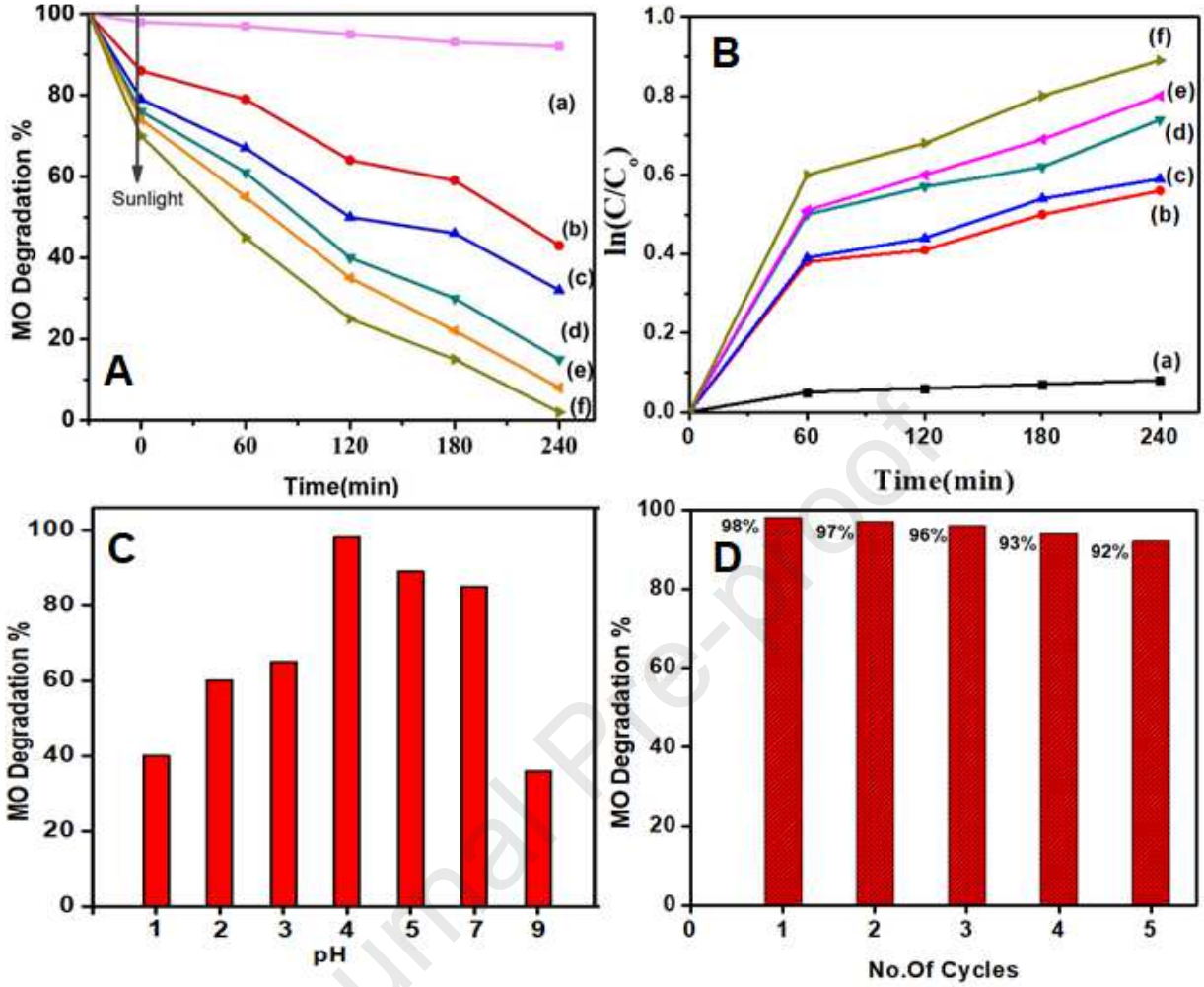

Figure 10. (A) Time course decaying profile, (B) Kinetic studies of the degradation of MO under sunlight by pristine oxides, binary and ternary nanocomposites; (a) pristine γ-Al_2O_3, (b) pure CuO, (c) pure α-Fe_2O_3, (d) CuO/γ-Al_2O_3, (e) α-Fe_2O_3/γ-Al_2O_3, (f) CuO/α-Fe_2O_3/γ-Al_2O_3 composites. (C) Comparison of photocatalytic degradation of MO by CuO/α-Fe_2O_3/γ-Al_2O_3 ternary nanocomposite at different pH values. (D) The reusability of CuO/α-Fe_2O_3/γ-Al_2O_3 ternary nanocomposite after degradation process.

3.2.1. Kinetic studies

The modified Langmuir-Hinshelwood model provides the pseudo-first-order kinetics for photocatalysis. Photocatalytic activity can be estimated by apparent rate constant (k_{app}) at

different light intensities. The first order kinetics determining that photoactivity is obtained by the equation given below [65].

$$\ln (C/C_o) = k_{app}\, t$$

Where C= concentration of solution at irradiation time t and C_o= initial concentration at t=0 and k_{app} is apparent rate constant. The change in ln (C_o/C) as a function of irradiation time are given in Figure 10B.

3.2.2. Influence of solution pH on dye degradation

In the degradation of organic dye, pH of the solution is considered to be key factor in photocatalysis experiment. Figure 10C indicated the impact of pH of the solution on the decolourization of MO. The ternary composite CuO/α-Fe_2O_3/γ-Al_2O_3 showed the maximal photocatalytic activity of 98.0% at low pH=4 of the solution whereas activity was found to be 40.0%, 60.0%, 65.0%, 89.0%, 85.0% and 36.0% at pH values of 1.0, 2.0, 3.0, 5.0, 7.0 and 9.0. The results indicated that the solution in lower pH (acidic conditions) favors increased photo reduction ability for MO than in alkaline media as in accordance with the literature. The dye degradation phenomena is closely related to pH of the solution which in turn effects the surface charge of adsorbents. In alkaline condition, the photocatalytic activity reduces because the catalyst surface becomes negatively charged and repels the dye molecules to absorb on the CuO/α-Fe_2O_3/γ-Al_2O_3 surface, thus suppressing the reduction rate of MO. Conversely, in acidic condition (low pH) surface of CuO/α-Fe_2O_3/γ-Al_2O_3 becomes highly protonated, providing the strong electrostatic attraction to the active and main molecules of MO and positively charged surface of CuO/α-Fe_2O_3/γ-Al_2O_3 which would result in increased photocatalytic activity of CuO/α-Fe_2O_3/γ-Al_2O_3 [66, 67].

3.2.3. Reusability and structure of the photocatalyst

The reusability of ternary CuO/α-Fe_2O_3/γ-Al_2O_3 nanocomposite is very essential for practical application. There is no such report on the long term durability of CuO/α-Fe_2O_3/γ-Al_2O_3 for MO photo reduction. The reusability of ternary CuO/α-Fe_2O_3/γ-Al_2O_3 hybrid structure was studied by repetitive photocatalytic detoxification of MO by ternary heterojunction under solar light for five cycles. Figure 10D illustrates that after five cycle's degradation rate of MO was not less than 92.0%. The slight decrease of the 6.0% is mainly due to filtration loss and fouling of catalyst [68]. The synthesized catalyst shows good stability, durability and reusability. Hence ternary composite CuO/α-Fe_2O_3/γ-Al_2O_3 has proved to be an efficient photo catalyst that prevent the environment from being polluted. Moreover, the ternary heterojunction (CuO/α-Fe_2O_3/γ-Al_2O_3) after the photocatalysis was subjected to XRD to evaluate the structural stability. The corresponding XRD spectra of recovered sample as shown in Figure 11 delineates that there is absolutely no change in peak position but there is slight decreases in peak intensity of CuO/α-Fe_2O_3/γ-Al_2O_3 compared to as prepared materials. These results suggests that crystal structure of the photo catalyst remains unchanged before and after photocatalysis which means that the internal structure of the catalyst remain same and will not break after catalytic process. Hence, prepared ternary heterojunction exhibits the excellent stability after degradation process.

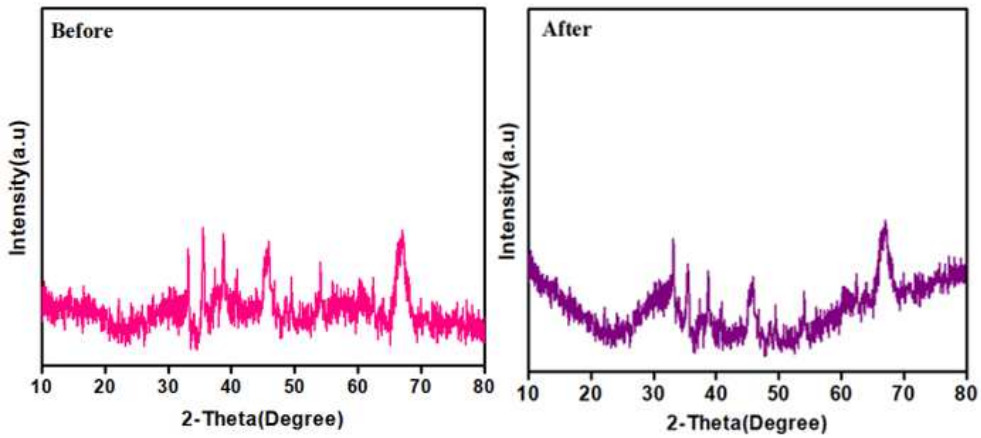

Figure 11. XRD profile of the ternary photo catalyst CuO/α-Fe_2O_3/γ-Al_2O_3 before and after photo-catalytic experiment.

3.2.4. Cascade electron transfer mechanism

To examine role of photo created active species involved in photocatalytic reaction and to explore the MO degradation, different scavenger such as ammonium oxalate (AO), $AgNO_3$, Tetra-butyl alcohol (TBA) and Benzoquinone (BQ) were employed as trapping agent for hole (h^+), electron (e^-), hydroxyl radical (OH) and superoxide radical ($O_2^{\bullet-}$), respectively. The photocatalytic activity of ternary nanocomposite reduced under visible light by hole scavenger as holes are important species. The photocatalytic activity negligibly decreases upon addition electron trapping agent. This slight decrease indicate that electron are not directly involved in degradation process. The hydroxyl radical (OH) scavenger implies that hydroxyl radical has effective role in degradation process. The superoxide radical ($O_2^{\bullet-}$) scavenging has largest effect on the decolorization of pollutant [60]. Moreover it is concluded that $O_2^{\bullet-}$ and hole plays an imperative role for the degradation of methyl orange under visible light. Figure 12 shows degradation % change in order of e^->OH>h^+> $O_2^{\bullet-}$ [69].

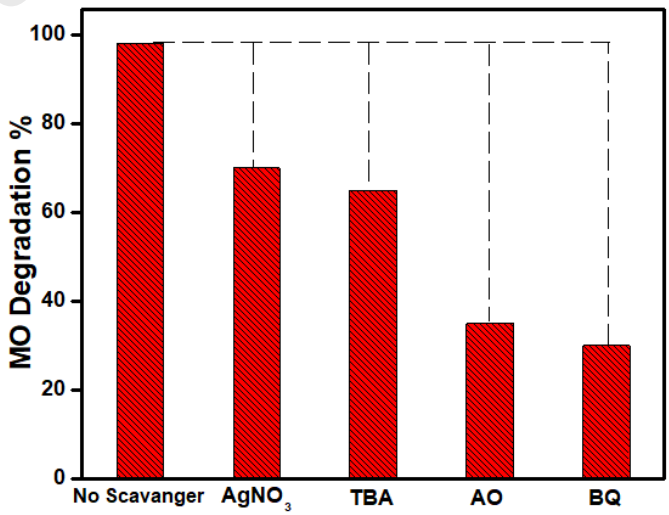

Figure 12. Controlled experiments of photocatalytic degradation of methyl orange using different trapping agents over CuO/α-Fe_2O_3/γ-Al_2O_3 ternary nanocomposite under visible light irradiation.

To analyze the charge migration between CuO, α-Fe_2O_3 and γ-Al_2O_3, the positions of CB(conduction band)and VB(valence band) were estimated by using following equations;

$$E_{VB} = \chi - E_e + 0.5E_g \quad \ldots\ldots\ldots\ldots\ldots (1)$$

$$E_{CB} = E_{VB} - E_g \quad \ldots\ldots\ldots\ldots\ldots (2)$$

Where E_e = free electron energy (4.5 eV), χ=Electronegativity

The value of χ for CuO, α-Fe_2O_3 and γ-Al_2O_3 is 5.79 eV [70], 5.84 eV [71] and 5.33 eV [11] respectively. The E_{CB} and E_{VB} of CuO were estimated to be +0.30eV/NHE and +2.1 eV/NHE whereas α-Fe_2O_3 were calculated as +0.36eV/NHE and +2.4 eV/NHE. The corresponding band alignment of ternary nanocomposite CuO/α-Fe_2O_3/γ-Al_2O_3 is shown in Figure 13. Consequently, the obtained results are used for the cascade transference of photo generated charge carriers in ternary hybrid structure which illustrate the photocatalytic process. From above results, it can be seen that although the conduction band potential of Al_2O_3 is higher than that of CuO and α-Fe_2O_3, but photo-induced electrons of CuO have ability to move to low lying defect level of γ-Al_2O_3 via α-Fe_2O_3. In the present study, amorphous γ-Al_2O_3 acts as electrons sink because amorphous materials are composed of large number of defect sites than crystalline structures. Thus, the migration of electrons to the low lying defect levels of amorphous γ-Al_2O_3 increases the separation of e^-/h^+ which in turns leads to enhanced the photo activity [72]

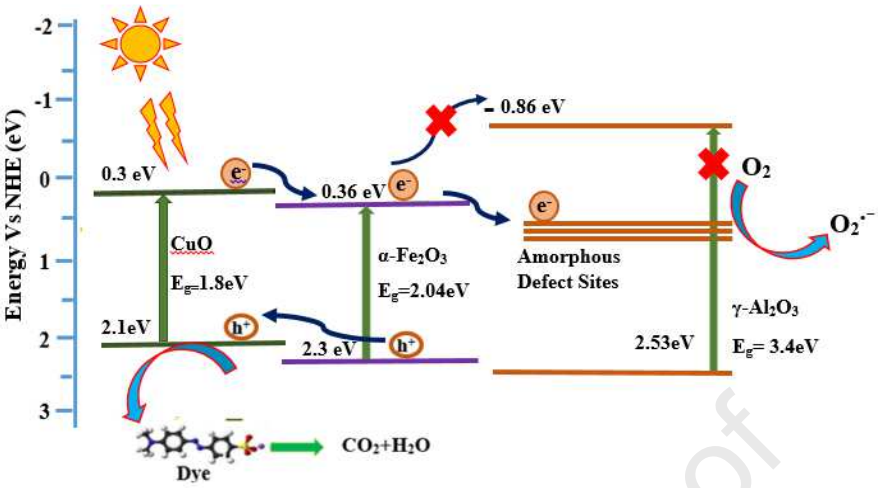

Figure 13. Energy band diagram of CuO/α-Fe_2O_3/γ-Al_2O_3 ternary nanocomposite for degradation of MO.

On the basis of experimental results and samples characterization, probable facile electron transfer route over CuO/α-Fe_2O_3/γ-Al_2O_3 ternary heterojunction under solar light illumination is manifested in Fig. 13. Firstly electrons in HOMO (VB) of CuO are moved to LOMO (CB) under sunlight irradiation. Now some of electron would migrate from conduction band (CB) of CuO to CB (conduction band) of α-Fe_2O_3 because the conduction band potential of CuO (+0.3) is lower than potential of α-Fe_2O_3 (+0.36) and then transfer to the defect sites of γ-Al_2O_3, creating the cascade transport pathway. Some of the electron in the CB of CuO would reduce O_2 adsorbed on the surface of CuO to produce radicals $^{\bullet}O^{2-}$. This facile stepwise electron transfer route leads to increase the quantum efficiency and suppress the e-h recombination. Now secondly, O_2 absorb on the surface of CuO/α-Fe_2O_3/γ-Al_2O_3 nanocomposite can capture the photo induced electrons on the α-Fe_2O_3 and on the defect sites of γ-Al_2O_3 and activate molecular oxygen to produce $O_2^{\cdot-}$. The $O_2^{\cdot-}$ reacts with H_2O to form hydroxyl radical ($OH^{\cdot}$) which is considered to be an important oxidant in oxidation phenomena. Finally, the toxic organic dye (MO) reacts with $O_2^{\cdot-}$, holes and degrades with release of CO_2 and H_2O. It is noteworthy that during photocatalytic reaction $O_2^{\cdot-}$

and holes are key species which is confirmed by the experimental results [17, 18, 28, 73-75]. Fundamental stages involved in redox reaction of CuO/α-Fe_2O_3/γ-Al_2O_3 nanocomposite and organic species are illustrated by chemical equations as follow;

$h\upsilon + (CuO/\alpha\text{-}Fe_2O_3/\gamma\text{-}Al_2O_3) \rightarrow (CuO/\alpha\text{-}Fe_2O_3/\gamma\text{-}Al_2O_3) + h_{vb}^{+} + e_{cb}^{-}$

$CuO\ (e_{cb}^{-}) \rightarrow \alpha\text{-}Fe_2O_3$

$\alpha\text{-}Fe_2O_3\ (e_{cb}^{-}) \rightarrow \gamma\text{-}Al_2O_3\ (e_{cb}^{-}$ defect sites)

$\alpha\text{-}Fe_2O_3\ (e_{cb}^{-}) + \gamma\text{-}Al_2O_3\ (e_{cb}^{-}) + O_2 \rightarrow O_2^{\bullet -}$

$CuO\ (h_{vb}^{+}) + OH^{-} \rightarrow CuO + OH^{\bullet}$

$O_2^{\bullet -} + (H_2O) \rightarrow H_2O_2$

$H_2O_2 \rightarrow OH^{\bullet}$

h^{+} + Methyl Orange → Oxidized Product

$O_2^{\bullet -}$ + Methyl Orange → Oxidized Product

4. Conclusions

In summary, facile and cost effective wet chemical method was adopted for the fabrication of ternary CuO/α-Fe_2O_3/γ-Al_2O_3 heterojunction with the same concentration of each component. XRD manifested the porous nature of γ-Al_2O_3 in all prepared samples. The recycling experiments illustrate that the ternary hybrid composite possessed excellent stability after five cycles without any change in its structure. The efficacy of pure, binary and ternary nanocomposites for degradation of MO was studied and CuO/α-Fe_2O_3/γ-Al_2O_3 nanocomposite reveals the maximum photocatalytic performance. The excellent visible light photocatalytic performance of CuO/α-Fe_2O_3/γ-Al_2O_3 hybrid structure can be accredited to the synergistic cooperation between CuO, α-Fe_2O_3, and γ-Al_2O_3 nanoparticles in the hybrid structure that improve light absorption capacity and hindering e-h recombination. Mullikan electronegativity

theory was employed to estimate the conduction and valance band position of CuO, α-Fe_2O_3 and γ-Al_2O_3 in ternary hybrid system. The charge transfer behavior of pure γ-Al_2O_3 and ternary composite CuO/α-Fe_2O_3/γ-Al_2O_3 were also investigated by linear sweep voltammetry and cyclic voltammetry. LSV results suggested CuO/α-Fe_2O_3/γ-Al_2O_3 showed current density of 69 μA/cm^2 at a potential of 1.76 V which is about 4.3 times larger than that of pristine γ-Al_2O_3 (16 μA/cm^2). N_2 adsorption-desorption isotherms delineates that ternary nanocomposite CuO/α-Fe_2O_3/γ-Al_2O_3 exhibit large surface area (56.2 cm^2/g) as compared to pristine γ-Al_2O_3. The current study shed the light on the imperative role of defects in γ-Al_2O_3. Defects sites of γ-Al_2O_3 can trap the photo generated electron of CuO via mediated α-Fe_2O_3 and decreases the recombination of charge carriers due to their intimate contact, strong interfacial hybridization and proficient charge transfer capacity. Overall, this study will create an interest in researching for new and novel ternary hybrid nanostructures.

Conflict of Interest.

There are no conflicts of interest to declare.

Acknowledgments

This research work was supported by Higher Education Commission of Pakistan (NRPU research grant 3660), International Islamic University Pakistan (IIUI), Pakistan Institute of Engineering and Applied Sciences (PIEAS). We are highly grateful to NUST, NCP, PIEAS, AIOU, UOP, IST and GCU Pakistan for analysis.

References

[1]. Yang, Y., Zheng, Z., Yang, M., Chen, J., Li, C., Zhang, C., & Zhang, X. (2020). In-situ fabrication of a spherical-shaped Zn-Al hydrotalcite with BiOCl and study on its enhanced

photocatalytic mechanism for perfluorooctanoic acid removal performed with a response surface methodology. *Journal of Hazardous Materials*, 399, 123070.

[2]. Wang, Y., Yu, L., Wang, R., Wang, Y., & Zhang, X. (2020). A novel cellulose hydrogel coating with nanoscale Fe0 for Cr (VI) adsorption and reduction. *Science of the Total Environment*, 726, 138625.

[3]. Wang, Y., Yu, L., Wang, R., Wang, Y., & Zhang, X. (2020). Reactivity of carbon spheres templated Ce/$LaCo_{0.5}Cu_{0.5}O_3$ in the microwave induced H_2O_2 catalytic degradation of salicylic acid: Characterization, kinetic and mechanism studies. *Journal of Colloid and Interface Science*. 574, 74-86

[4]. Yang, Y., Zheng, Z., Ji, W., Xu, J., & Zhang, X. (2020). Insights to perfluorooctanoic acid adsorption micro-mechanism over Fe-based metal organic frameworks: Combining computational calculation with response surface methodology. *Journal of Hazardous Materials*, 395, 122686.

[5]. Wang, Y., Wang, R., Yu, L., Wang, Y., Zhang, C., & Zhang, X. (2020). Efficient reactivity of $LaCu_{0.5}Co_{0.5}O_3$ perovskite intercalated montmorillonite and g-C_3N_4 nanocomposites in microwave-induced H_2O_2 catalytic degradation of bisphenol A. *Chemical Engineering Journal*, *401*, 126057.

[6]. Chen, J., Zhang, X., Bi, F., Zhang, X., Yang, Y., & Wang, Y. (2020). A facile synthesis for uniform tablet-like TiO_2/C derived from Materials of Institut Lavoisier-125 (Ti)(MIL-125 (Ti)) and their enhanced visible light-driven photodegradation of tetracycline. *Journal of Colloid and Interface Science*. 571, 275-284

[7]. Iqbal, A., Sajjad, S., & Leghari, S. A. K. (2018). Low cost graphene oxide modified alumina nanocomposite as solar light induced photocatalyst. *ACS Applied Nano Materials*, *1*(9), 4612-4621.

[8]. Payra, S., Challagulla, S., Bobde, Y., Chakraborty, C., Ghosh, B., & Roy, S. (2019). Probing the photo-and electro-catalytic degradation mechanism of methylene blue dye over ZIF-derived ZnO. *Journal of Hazardous Materials*, *373*, 377-388.

[9]. Chen, J., Zhang, X., Shi, X., Bi, F., Yang, Y., & Wang, Y. (2020). Synergistic effects of octahedral TiO_2-MIL-101 (Cr) with two heterojunctions for enhancing visible-light photocatalytic degradation of liquid tetracycline and gaseous toluene. *Journal of Colloid and Interface Science*. 579, 37-49

[10]. Gulshan, F., & Okada, K. (2013). Preparation of alumina–iron oxide compounds by coprecipitation method and its characterization. *American Journal of Materials Science and Engineering*, *1*(1), 6-11.

[11]. Balamurugan, S., Balu, A. R., Narasimman, V., Selvan, G., Usharani, K., Srivind, J., ... & Nagarethinam, V. S. (2018). Multi metal oxide CdO–Al_2O_3–NiO nanocomposite—synthesis, photocatalytic and magnetic properties. *Materials Research Express*, *6*(1), 015022.

[12]. Wang, Y., Yu, L., Wang, R., Wang, Y., & Zhang, X. (2020). Microwave catalytic activities of supported perovskite catalysts MOx/LaCo0. 5Cu0. 5O3@ CM (M= Mg, Al) for salicylic acid degradation. *Journal of Colloid and Interface Science*, *564*, 392-405.

[13]. Leow, W. R., Ng, W. K. H., Peng, T., Liu, X., Li, B., Shi, W., ... & Mathews, N. (2017). Al_2O_3 surface complexation for photocatalytic organic transformations. *Journal of the American Chemical Society*, *139*(1), 269-276.

[14]. Samain, L., Jaworski, A., Edén, M., Ladd, D. M., Seo, D. K., Garcia-Garcia, F. J., & Häussermann, U. (2014). Structural analysis of highly porous γ-Al_2O_3. *Journal of Solid State Chemistry*, *217*, 1-8.

[15]. Chen, L. C., Tsai, F. R., & Huang, C. M. (2005). Photocatalytic decolorization of methyl orange in aqueous medium of TiO_2 and Ag–TiO_2 immobilized on γ-Al_2O_3. *Journal of Photochemistry and Photobiology A: Chemistry*, *170*(1), 7-14.

[16]. Saravanan, R., Karthikeyan, S., Gupta, V. K., Sekaran, G., Narayanan, V., & Stephen, A. J. M. S. (2013). Enhanced photocatalytic activity of ZnO/CuO nanocomposite for the degradation of textile dye on visible light illumination. *Materials Science and Engineering: C*, *33*(1), 91-98.

[17]. Lai, S. H., Chen, Y. B., Li, N., Su, H., & Guo, S. H. (2018). Novel g-C_3N_4 wrapped γ-Al_2O_3 microspheres heterojunction for efficient photocatalytic application under visible light irradiation. *Journal of Materials Science: Materials in Electronics*, *29*(6), 4509-4516.

[18]. Li, F. T., Zhao, Y., Hao, Y. J., Wang, X. J., Liu, R. H., Zhao, D. S., & Chen, D. M. (2012). N-doped P25 TiO_2–amorphous Al_2O_3 composites: One-step solution combustion preparation and enhanced visible-light photocatalytic activity. *Journal of Hazardous Materials*, *239*, 118-127.

[19]. Murali, D. S., Kumar, S., Choudhary, R. J., Wadikar, A. D., Jain, M. K., & Subrahmanyam, A. (2015). Synthesis of Cu_2O from CuO thin films: Optical and electrical properties. *AIP Advances*, *5*(4), 047143.

[20]. Sun, S., Sun, M., Kong, Y., Fang, Y., & Yao, Y. (2016). MoS_2 and graphene as dual, cocatalysts for enhanced visible light photocatalytic activity of Fe_2O_3. *Journal of Sol-Gel Science and Technology*, *80*(3), 719-727.

[21]. Zhang, X., Yang, Y., Song, L., Wang, Y., He, C., Wang, Z., & Cui, L. (2018). High and stable catalytic activity of Ag/Fe_2O_3 catalysts derived from MOFs for CO oxidation. *Molecular Catalysis*, *447*, 80-89.

[22]. Nagarjuna, R., Challagulla, S., Ganesan, R., & Roy, S. (2017). High rates of Cr (VI) photoreduction with magnetically recoverable nano-Fe_3O_4@ Fe_2O_3/Al_2O_3 catalyst under visible light. *Chemical Engineering Journal*, *308*, 59-66.

[23]. Yang, Y., Dong, H., Wang, Y., Wang, Y., Liu, N., Wang, D., & Zhang, X. (2017). A facile synthesis for porous CuO/Cu_2O composites derived from MOFs and their superior catalytic performance for CO oxidation. *Inorganic Chemistry Communications*, *86*, 74-77.

[24]. Sajjad, S., Bano, T., Sajjad, A.K.L., (2017). Efficient visible light magnetic modified iron oxide photocatalysts. Ceramics International 43(17), 14672-14677.

[25]. Bahgat, M., Paek, M. K., & Pak, J. J. (2009). Reduction investigation of $WO_3/NiO/Fe_2O_3$ and synthesis of nanocrystalline ternary W–Ni–Fe alloy. *Journal of alloys and compounds*, *472*(1-2), 314-318.

[26]. Zhang, X., Zhang, X., Song, L., Hou, F., Yang, Y., Wang, Y., & Liu, N. (2018). Enhanced catalytic performance for CO oxidation and preferential CO oxidation over CuO/CeO_2 catalysts synthesized from metal organic framework: effects of preparation methods. *International Journal of Hydrogen Energy*, *43*(39), 18279-18288.

[27]. Bradu, C., Frunza, L., Mihalche, N., Avramescu, S. M., Neaţă, M., & Udrea, I. (2010). Removal of Reactive Black 5 azo dye from aqueous solutions by catalytic oxidation using CuO/Al_2O_3 and NiO/Al_2O_3. *Applied Catalysis B: Environmental*, *96*(3-4), 548-556.

[28]. Liu, S. J., Li, F. T., Li, Y. L., Hao, Y. J., Wang, X. J., Li, B., & Liu, R. H. (2017). Fabrication of ternary g-C_3N_4/Al_2O_3/ZnO heterojunctions based on cascade electron transfer toward molecular oxygen activation. *Applied Catalysis B: Environmental*, *212*, 115-128.

[29]. Wahab, R., Khan, F., & Al-Khedhairy, A. A. (2018). Hematite iron oxide nanoparticles: apoptosis of myoblast cancer cells and their arithmetical assessment. *RSC Advances*, *8*(44), 24750-24759.

[30]. Ashok, C. H., Rao, K. V., & Chakra, C. S. (2014). Structural analysis of CuO nanomaterials prepared by novel microwave assisted method. *Journal of Atoms and Molecules*, *4*(5), 803.

[31]. Suresh, S., Karthikeyan, S., & Jayamoorthy, K. (2016). FTIR and multivariate analysis to study the effect of bulk and nano copper oxide on peanut plant leaves. *Journal of Science: Advanced Materials and Devices*, *1*(3), 343-350.

[32]. Liu, W. J., Zeng, F. X., Jiang, H., Zhang, X. S., & Li, W. W. (2012). Composite Fe_2O_3 and ZrO_2/Al_2O_3 photocatalyst: preparation, characterization, and studies on the photocatalytic activity and chemical stability. *Chemical Engineering Journal*, *180*, 9-18.

[33]. Wu, H., Lin, S., Chen, C., Liang, W., Liu, X., & Yang, H. (2016). A new ZnO/rGO/polyaniline ternary nanocomposite as photocatalyst with improved photocatalytic activity. *Materials Research Bulletin*, *83*, 434-441.

[34]. Jabbar, S. M. (2016). Synthesis of CuO nano structure via sol-gel and precipitation chemical methods. *Al-Khwarizmi Engineering Journal*, *12*(4), 126-131.

[35]. Tadic, M., Trpkov, D., Kopanja, L., Vojnovic, S., & Panjan, M. (2019). Hydrothermal synthesis of hematite (α-Fe2O3) nanoparticle forms: Synthesis conditions, structure, particle shape analysis, cytotoxicity and magnetic properties. *Journal of Alloys and Compounds*, *792*, 599-609.

[36] Chu, T. P. M., Nguyen, N. T., Vu, T. L., Dao, T. H., Dinh, L. C., Nguyen, H. L., ... & Pham, T. D. (2019). Synthesis, Characterization, and Modification of Alumina Nanoparticles for Cationic Dye Removal. *Materials*, *12*(3), 450.

[37] Hosseini, S. A., Niaei, A., & Salari, D. (2011). Production of γ-Al_2O_3 from Kaolin. *Open Journal of Physical Chemistry*, *1*(02), 23.

[38] Mahinroosta, M., & Allahverdi, A. (2018). Production of nanostructured γ-alumina from aluminum foundry tailing for catalytic applications. *International Nano Letters*, *8*(4), 255-261.

[39]. Farahmandjou, M., & Soflaee, F. (2014). Low temperature synthesis of α-Fe_2O_3 nano-rods using simple chemical route. *Journal of Nanostructure*, 4, 413-418.

[40]. Justus, J. S., Roy, S. D. D., & Raj, A. M. E. (2016). Synthesis and characterization of hematite nanopowders. *Materials Research Express*, *3*(10), 105037.

[41]. Ubale, A. U., & Belkhedkar, M. R. (2015). Size dependent physical properties of nanostructured α-Fe_2O_3 thin films grown by successive ionic layer adsorption and reaction method for antibacterial application. *Journal of Materials Science & Technology*, *31*(1), 1-9.

[42]. Abdulah, H. I., Farhan, A. M., & Ali, A. J. (2015). Photo-synthesis of nanosized α–Fe_2O_3. *Journal of Chemical and Pharmaceutical Research*, *7*(6), 588-591.

[43]. Siahpoosh, S. M., Salahi, E., Hessari, F. A., & Mobasherpour, I. (2017). Facile synthesis of γ-Alumina nanoparticles via the sol gel method in presence of various solvents. *Sigma: Journal of Engineering & Natural Sciences/Mühendislik ve Fen Bilimleri Dergisi*, *35*(3).

[44]. Sharma, A., & Lee, B. K. (2016). Integrated ternary nanocomposite of TiO_2/NiO/reduced graphene oxide as a visible light photocatalyst for efficient degradation of o-chlorophenol. *Journal of environmental management*, *181*, 563-573.

[45]. Padil, V. V. T., & Černík, M. (2013). Green synthesis of copper oxide nanoparticles using gum karaya as a biotemplate and their antibacterial application. *International journal of nanomedicine*, *8*, 889.

[46]. Yu, Q., Huang, H., Chen, R., Wang, P., Yang, H., Gao, M., ... & Ye, Z. (2012). Synthesis of CuO nanowalnuts and nanoribbons from aqueous solution and their catalytic and electrochemical properties. *Nanoscale*, *4*(8), 2613-2620.

[47]. Velusamy, T., Liguori, A., Macias□Montero, M., Padmanaban, D. B., Carolan, D., Gherardi, M., ... & Mariotti, D. (2017). Ultra□small CuO nanoparticles with tailored energy□band diagram synthesized by a hybrid plasma□liquid process. *Plasma Processes and Polymers*, *14*(7), 1600224.

[48]. Farahmandjou, M., & Soflaee, F. (2015). Synthesis and characterization of α-Fe_2O_3 nanoparticles by simple co-precipitation method. *Physical Chemistry Research*, *3*(3), 191-196.

[49]. Mahmoud, Z. H. (2017). The magnetic properties of alpha phase for iron oxide NPs that prepared from its salt by novel photolysis method. *Journal of Chemical and Pharmaceutical Research*, *9*(8), 29-33.

[50]. Renuka, N. K., Shijina, A. V., Praveen, A. K., & Aniz, C. U. (2014). Redox properties and catalytic activity of CuO/γ-Al_2O_3 meso phase. *Journal of Colloid and Interface Science*, *434*, 195-200.

[51]. Taufik, A., & Saleh, R. (2017, January). Combination of ternary Fe_3O_4/TiO_2/CuO nanocomposites and nanographene platelets: High performance photo and sonocatalysis. In *AIP Conference Proceedings* (Vol. 1788, No. 1, p. 030037). AIP Publishing LLC.

[52]. Wei, Y., Zhang, Y., Geng, W., Su, H., Long, M., (2019). Efficient bifunctional piezocatalysis of Au/$BiVO_4$ for simultaneous removal of 4-chlorophenol and Cr (VI) in water. *Applied Catalysis B: Environmental*, 259, 118084.

[53]. Jamila, G. S., Sajjad, S., Leghari, S. A. K., & Mahmood, T. (2020). Role of nitrogen doped carbon quantum dots on CuO nano-leaves as solar induced photo catalyst. *Journal of Physics and Chemistry of Solids*, *138*, 109233.

[54]. Casillas, J. E., Campa-Molina, J., Tzompantzi, F., Carbajal Arízaga, G. G., López-Gaona, A., Ulloa-Godínez, S., ... & Barrera, A. (2020). Photocatalytic Degradation of Diclofenac Using Al_2O_3-Nd_2O_3 Binary Oxides Prepared by the Sol-Gel Method. *Materials*, *13*(6), 1345.

[55]. Naghib, S. M., Zare, Y., & Rhee, K. Y. (2020). A facile and simple approach to synthesis and characterization of methacrylated graphene oxide nanostructured polyaniline nanocomposites. *Nanotechnology Reviews*, *9*(1), 53-60.

[56]. Khan, M. M., Ansari, S. A., Khan, M. E., Ansari, M. O., Min, B. K., & Cho, M. H. (2015). Visible light-induced enhanced photoelectrochemical and photocatalytic studies of gold decorated SnO_2 nanostructures. *New Journal of Chemistry*, *39*(4), 2758-2766.

[57]. Shafi, A., Ahmad, N., Sultana, S., Sabir, S., & Khan, M. Z. (2019). Ag_2S-Sensitized NiO–ZnO Heterostructures with Enhanced Visible Light Photocatalytic Activity and Acetone Sensing Property. *ACS Omega*, *4*(7), 12905-12918.

[58]. Balu, S., Velmurugan, S., Palanisamy, S., Chen, S. W., Velusamy, V., Yang, T. C., & El-Shafey, E. S. I. (2019). Synthesis of α-Fe_2O_3 decorated g-C_3N_4/ZnO ternary Z-scheme photocatalyst for degradation of tartrazine dye in aqueous media. *Journal of the Taiwan Institute of Chemical Engineers*, *99*, 258-267.

[59]. Bi, F., Zhang, X., Chen, J., Yang, Y., & Wang, Y. (2020). Excellent catalytic activity and water resistance of UiO-66-supported highly dispersed Pd nanoparticles for toluene catalytic oxidation. *Applied Catalysis B: Environmental*, *269*, 118767.

[60]. Shi, X., Zhang, X., Bi, F., Zheng, Z., Sheng, L., Xu, J., ... & Yang, Y. (2020). Effective toluene adsorption over defective UiO-66-NH2: An experimental and computational exploration. *Journal of Molecular Liquids*, *316*, 113812.

[61]. Mageshwari, K., Nataraj, D., Pal, T., Sathyamoorthy, R., & Park, J. (2015). Improved photocatalytic activity of ZnO coupled CuO nanocomposites synthesized by reflux condensation method. *Journal of Alloys and Compounds*, *625*, 362-370.

[62]. Mishra, M., & Chun, D. M. (2015). α-Fe_2O_3 as a photocatalytic material: A review. *Applied Catalysis A: General*, *498*, 126-141.

[63]. Sajjad, A.K.L., Shamaila, S., Iqbal, A., 2018. ZnO/WO_3 nanostructure as an efficient visible light catalyst, *Ceramics International*. 44(8), 9364-9371

[64]. Taufik, A., Albert, A., & Saleh, R. (2017). Sol-gel synthesis of ternary $CuO/TiO_2/ZnO$ nanocomposites for enhanced photocatalytic performance under UV and visible light irradiation. *Journal of Photochemistry and Photobiology A: Chemistry*, *344*, 149-162.

[65]. Li, F. T., Xue, Y. B., Li, B., Hao, Y. J., Wang, X. J., Liu, R. H., & Zhao, J. (2014). Precipitation synthesis of mesoporous photoactive Al_2O_3 for constructing g-C_3N_4-based heterojunctions with enhanced photocatalytic activity. *Industrial & Engineering Chemistry Research*, *53*(50), 19540-19549.

[66]. Sajjad, A. K. L., Shamaila, S., Tian, B., Chen, F., & Zhang, J. (2010). Comparative studies of operational parameters of degradation of azo dyes in visible light by highly efficient WO_x/TiO_2 photocatalyst. *Journal of Hazardous Materials*, *177*(1-3), 781-791.

[67]. Yuan, X., Cheng, X., Jing, Q., Niu, J., Peng, D., Feng, Z., & Wu, X. (2018). $ZnO/ZnAl_2O_4$ nanocomposite with 3D sphere-like hierarchical structure for photocatalytic reduction of aqueous Cr (VI). *Materials*, *11*(9), 1624.

[68]. Sajjad, A.K.L., Shamaila, S., Zhang, J., (2014). A time saving and cost effective route for metal oxides activation, *RSC Advances*, 4(10), 5248-5253.

[69] Pan, Y., Su, H., Zhu, Y., Molamahmood, H.V., Long, M., (2018). CaO_2 based Fenton-like reaction at neutral pH: Accelerated reduction of ferric species and production of superoxide radicals. *Water Research*, 145, 731-740.

[70]. Yu, Z., Moussa, H., Liu, M., Schneider, R., Moliere, M., & Liao, H. (2019). Heterostructured metal oxides-ZnO nanorods films prepared by SPPS route for photodegradation applications. *Surface and Coatings Technology*, *375*, 670-680.

[71]. Lakhera, S. K., Watts, A., Hafeez, H. Y., & Neppolian, B. (2018). Interparticle double charge transfer mechanism of heterojunction α-Fe2O3/Cu2O mixed oxide catalysts and its visible light photocatalytic activity. *Catalysis Today*, *300*, 58-70.

[72]. Yadav, S., Mittal, A., Sharma, S., Kumari, K., Chauhan, N. S., & Kumar, N. (2020). Low temperature synthesized ZnO/Al_2O_3 nano-composites for photocatalytic and antibacterial applications. *Semiconductor Science and Technology*, *35*(5), 055008.

[73]. Li, F. T., Liu, S. J., Xue, Y. B., Wang, X. J., Hao, Y. J., Zhao, J., ... & Zhao, D. (2015). Structure Modification Function of g□C_3N_4 for Al_2O_3 in the In Situ Hydrothermal Process for Enhanced Photocatalytic Activity. *Chemistry–A European Journal*, *21*(28), 10149-10159.

[74]. Ismail, A. A., Abdelfattah, I., Atitar, M. F., Robben, L., Bouzid, H., Al-Sayari, S. A., & Bahnemann, D. W. (2015). Photocatalytic degradation of imazapyr using mesoporous Al_2O_3–TiO_2 nanocomposites. *Separation and Purification Technology*, *145*, 147-153.

[75]. Sajjad, S., Sajjad, A.K.L., Shaheen, S., Iqbal, A., Noor, S., Sughra, G., Ali, U., (2017) A cost effective and eco-friendly green route for fabrication of efficient graphene nanosheets photocatalyst, *Journal of Environmental Chemical Engineering*, 5 (6), 5770-5776.

Highlights

- CuO/α-Fe_2O_3/γ-Al_2O_3 ternary nanocomposite is utilized as visible photocatalyst.
- The CuO/α-Fe_2O_3/γ-Al_2O_3 hybrid structure is accredited to synergistic interaction.
- The hybrid structure improve light absorption and repressed e-h recombination.
- Defects sites of γ-Al_2O_3 trap the photo generated electron of CuO via α-Fe_2O_3.
- Efficacy is due to strong interfacial hybridization and charge transfer capacity.

Declaration of interests

☒ The authors declare that they have no known competing financial interests or personal relationships that could have appeared to influence the work reported in this paper.

☐The authors declare the following financial interests/personal relationships which may be considered as potential competing interests:

Dr. Shamaila Sajjad
Associate Professor International Islamic University, Islamabad, Pakistan

E-mail: shalisajjad@yahoo.com

Phone No. 0092519019813